ELSEVIER

Journal of Molecular Catalysis A: Chemical 119 (1997) 335–348

JOURNAL OF MOLECULAR CATALYSIS A: CHEMICAL

Model parametric Hamiltonians and bonding theoretical tools in simulation of catalytic reaction steps. Hydrotreatment of oil components

Fernando Ruette [a,*], Flor M. Poveda [b], Anibal Sierraalta [a], Morella Sánchez [c], Eloy N. Rodríguez-Arias [d]

[a] *Centro de Química, Laboratorio de Química Computacional, Instituto Venezolano de Investigaciones Científicas (IVIC), Apartado 21827, Caracas 1020-A, Venezuela*

[b] *Grupo de Química Teórica, Facultad de Ciencias, Universidad Nacional de Colombia, Bogotá, Colombia*

[c] *Departamento de Química, IUT, Apartado 40437, Caracas, Venezuela*

[d] *Departamento de Química, Laboratorio de Modelaje en Catálisis, Universidad Simón Bolívar, Apartado 89000, Caracas 1080-A, Venezuela*

Received 4 June 1996; accepted 8 July 1996

Abstract

Quantum chemistry calculations of hydrocarbons components and hydrogen have been carried out using model surface adsorption sites on aggregates and model parametric Hamiltonians. Bader's topological analysis of the charge density in the valence region is used to describe the adsorption site on which reactions may occur. A description of the adsorbate and surface bindings with diatomic binding energies (DBE) and orbital interactions are presented. Chemisorption and hydrogenation reactions of molecular fragments that are intermediates in hydrocarbon formation on a nickel aggregate were calculated. Also, the growing of hydrocarbon chains and the building of carbonaceous filaments were studied. The modeling of hydrogen dissociation on HDS catalyst was analyzed. In addition, the hydrogenation step of the HDN reaction on a modeled MoS_2 catalyst, employing pyridine as model molecule, is presented.

Keywords: Hydrogenation reactions; Nickel catalyst; Model Hamiltonians; Bader's theory; Molybdenum sulphide; H_2 dissociation; HDN; HDS; Semiempirical methods

1. Introduction

Crude oil is mainly composed of paraffins, cycloparaffins, aromatics, and in smaller proportion, hydrocarbons that contain nitrogen, oxygen, and sulfur. Traces of vanadium, nickel, and iron are in some cases present as organometallic compounds.

In the treatment of oil components, hydrogen is one of the most used compounds to produce new materials. It is employed to eliminate, from oil, some elements that are air contaminants and poisons of catalysts used in the reforming processes. Several reactions of great importance in petrochemical processes are related to hydro-

* Corresponding author.

PII S1381-1169(96)00496-7

gen, for example: hydrogenation, dehydrogenation, hydrodesulfurization, hydrodenitrogenation, hydrodeoxygenation, hydrocraking, hydrodealkylation, hydrodemetalization, coal liquefaction, etc. The understanding of these reactions requires the knowledge of several steps in which one of the most important is the dissociation of hydrogen.

Previous calculations [1–4] using modeled adsorption sites were carried out to simulate the chemisorption of hydrogen atoms, physisorption, dissociation and diffusion of a H_2 molecule, interaction between adsorbates, variation of surface properties with the coverage, changes of electronic spectra upon chemisorption, effects of charge density in the reactivity of the adsorption site, etc. All of these processes have been successfully studied with MINDO/SR method [5] and good correlations with experimental results have been found [6].

In this work we model several steps for reactions on transition metals in which hydrocarbons and/or hydrogen are present. The theoretical basis of the computational tools used here is also briefly reviewed.

2. Theoretical foundations

2.1. Model Hamiltonians

For molecules of large size and complex systems that contain transition metals, model Hamiltonians can be of great significance in the estimation of molecular properties. Ab initio evaluations of potential energy surfaces easily reach impractical limits of computer time and disk space, even for chemical reactions with small molecules.

Parametric model Hamiltonians can be defined by means of simulation techniques [7] or by generalized least squares methods [8]. A more detailed discussion of the foundations of these methods is presented elsewhere [9,10]. Nevertheless, a brief outline of the theory is given here. A parametric Hamiltonian (semiempirical Hamiltonian), H_{smp}, of n-body system can be represented in terms of a family (F) of Hamiltonians. The closest H_{smp} to the exact Hamiltonian (H_{exa}) is determined by the minimization of the distance, $\|\cdot\|$ between H_{exa} and H_{smp}. That is,

$$\min\|H_{\mathrm{exa}} - H_{\mathrm{smp}}\| = \min\left(\sum_{i,j}|H_{\mathrm{exa}}^{ij} - H_{\mathrm{smp}}^{ij}|^2\right)^{1/2} \qquad H_{\mathrm{smp}} \in F \tag{1}$$

where $H_{\mathrm{exa}}^{ij} = \langle\Psi_i|H_{\mathrm{exa}}|\Psi_i\rangle$ and H_{smp}^{ij} are functionals. The first functionals depend on the wavefunctions $\{\Psi_j\}$, while the second-ones are, in general, defined by parametric expressions.

One practical manner of evaluating these functionals and parameters is by considering energy differences between distinct systems or between different states; for example, from the dissociation of a diatomic molecule AB. If the minimization is considered only with respect to the energy mean value of selected A, B, and AB states, the following expression results,

$$\min\|H_{\mathrm{exa}}^{\mathrm{AB}} - H_{\mathrm{smp}}^{\mathrm{AB}}\| = \min\left(\sum_{i}|\mathrm{BE}_{\mathrm{exa}_i}^{\mathrm{AB}} - \mathrm{BE}_{\mathrm{smp}_i}^{\mathrm{AB}}|^2\right)^{1/2} \qquad H_{\mathrm{smp}} \in F \tag{2}$$

where,

$$\mathrm{BE}_i^{\mathrm{AB}} = \langle\Psi_i^{\mathrm{AB}}|H^{\mathrm{AB}}|\Psi_i^{\mathrm{AB}}\rangle - \langle\Psi^{\mathrm{A}}|H^{\mathrm{A}}|\Psi^{\mathrm{A}}\rangle - \langle\Psi^{\mathrm{B}}|H^{\mathrm{B}}|\Psi^{\mathrm{B}}\rangle \tag{3}$$

In practice, some $\mathrm{BE}_i^{\mathrm{AB}}$ are known, and in most of the cases only the ground state has been determined.

MINDO/SR [5] (a modified version of MINDO/3 [11] for transition metals) is a method based on simulation techniques using special functionals for transition metals. The parametrization was carried out to reproduce experimental dissociation energies and equilibrium bond distances for the ground state of diatomic molecules. A similar method has been

recently developed considering effective core potentials, analytic calculations of integrals, and the use of Gaussian functions [10].

2.2. Analysis of binding energies of local interactions

The evaluation of interactions between adsorbate–surface, surface–surface and adsorbate–adsorbate atoms is fundamental in the understanding of elementary steps that occur in catalytic processes: chemisorption of species, bond activation, surface reactions, diffusion, surface reconstruction, etc. Total diatomic energies (TDE) [12] and total Mulliken bond orders (TMBO) [13] have the tendency to be larger for multi-center coordinations than for single ones, even in cases in which the former present smaller binding interactions than the latter.

A new theoretical tool, diatomic binding energy (DBE) [14], allows an approximate evaluation of the interaction energy between atoms A and B in a molecular system. This variable is defined as:

$$\mathrm{DBE(A{-}B)} = \varepsilon_{AB} + f_A(\mathrm{A{-}B})\Delta\varepsilon_A + f_B(\mathrm{A{-}B})\Delta\varepsilon_B \quad (4)$$

where the ε_{AB} term corresponds to the diatomic energy between atoms A and B; $\Delta\varepsilon_A$ is the difference between the monoatomic energy and the energy of the free atom A ($\Delta\varepsilon_A = \varepsilon_A - \varepsilon_A^o$); and $f_A(\mathrm{A{-}B})$ is a factor ($0 \le f_A(\mathrm{A{-}B}) \le 1$) evaluated as:

$$f_A(\mathrm{A{-}B}) = |\varepsilon_{AB}| \Big/ \sum_{(C \neq A)} |\varepsilon_{AC}| \quad (5)$$

A simple picture of the DBE(A–B) variable for a diatomic molecule A–B is given in Fig. 1. The bond energy between two atoms has three components: one due to interactions between A and B atoms (ε_{AB}) and two due to energy changes of the involved atoms ($\Delta\varepsilon_A$ and $\Delta\varepsilon_B$). This definition obeys the condition that the total binding energy of a molecular system can be expressed as the sum of DBEs between all pairs of atoms. In addition, this formalism can be easily extended to ab initio SCF approaches by expressing three- and four-center terms as a sum of diatomic ones [15].

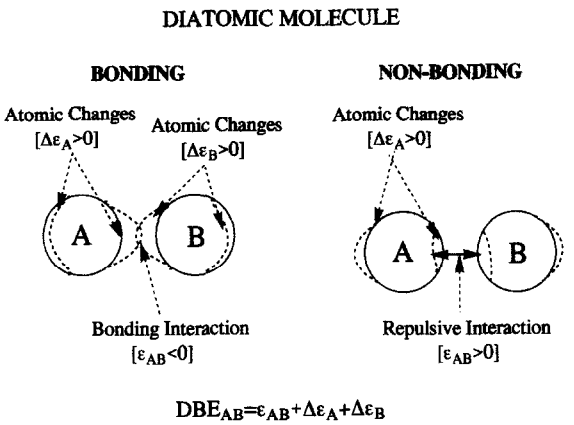

Fig. 1. Schematic picture of diatomic binding energy (DBE) components.

2.3. Analysis of local charge distribution

Characterization of chemical bonds and the local congregation or reduction of the electronic density in the valence region can be derived from the topological properties of $\rho(r)$ and Laplacian of $\rho(r)$ ($\Delta\rho(r)$), as has been established by Bader et al. [16] for molecular systems. The local critical points of $\Delta\rho(r)$ at the valence shell charge concentration (VSCC) of an atom in a molecule can be used to analyze the physical basis of the Lewis acid–base reaction model [16,17]. Very important applications to organic molecules [18] and to metallic systems that modeled catalytic surfaces [19] have been applied recently.

As mentioned at the beginning, the most accurate full-electron calculations for transition metals are impractical and very troublesome. Therefore, the use of effective core potentials (ECP) has been popularized for transition metals. Several articles have been published for the application of topological properties of $\rho(r)$ and $\Delta\rho(r)$ calculated from model Hamiltonians using different effective core potentials [20,21].

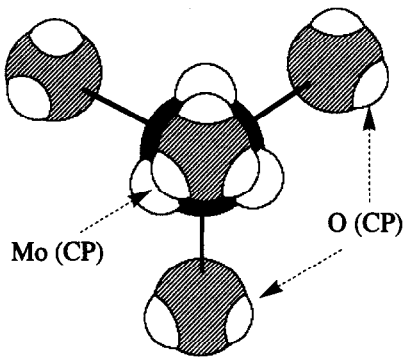

Fig. 2. Representation of electronic charge maxima at the atom valence shells ((3–3) critical points (CP)) for the MoO_4^{2-} molecule. White half-spheres correspond to CP. The dark central sphere represents the Mo atom and the dashed ones are the O atoms.

In recent papers Sierraalta and Ruette [20,21] have evaluated the topological properties of $\rho(r)$ and $\Delta\rho(r)$ at the bond and at the valence regions for molybdenum compounds. The results showed that semi-core approaches for ECP are able to reproduce, in a qualitative way, the location of critical points and their relative values with respect to those obtained by the full-electron (FE) HF method.

For example, the location of valence electronic charge concentrations on MoO_4^{2-} [20] are depicted in Fig. 2. Note that the knowledge of specific sites on each atom can be very helpful in the determination of the correct pathway for bonding or non-bonding interactions. It is possible to consider numerous ways to orientate an adsorbate on a surface; however, only few of them will be efficient for bonding interactions. As we will show below, an adequate pathway for H_2 dissociation on MoS_2 can be predicted, using the topological analysis of the density.

3. Chemisorption, hydrogenation, and reactions of hydrocarbon fragments on a nickel catalyst

In hydrogenation and dehydrogenation reactions of hydrocarbons, C–H bonds are formed or broken, respectively. Nickel finely divided and dispersed on different supports is normally used as catalyst for different processes of hydrocarbon hydrogenation, dehydrogenation, and synthesis. The catalyst particles, aggregates of very small size (few Å in diameter [22]), are, in general, highly effective catalysts because of their large surface accessible to reactants.

Several experimental articles report the existence of adsorbed CH_n ($n = 0$–3) fragments in the formation an decomposition of hydrocarbons on Ni catalyst [23–25] and on Ni crystal surfaces [26,27].

In this work, the catalyst is modeled by a little grain (tiny crystal) that contains 8 atoms of nickel in the first layer and 6 in the second (Ni_{14} cluster), see Fig. 3. All calculations were carried out with MINDO/SR method [5]. The interaction of CH_n ($n = 0$–3) fragments with different adsorption sites of a Ni cluster was evaluated using the DBE [14] for each bond. The formation of CH_n ($n = 1$–4) was evaluated from CH_n ($n = 0$–3) and adsorbed H atoms in the most stable sites. In addition, formation of C_mH_n hydrocarbons were also calculated from the interaction of several fragments.

3.1. The most stable adsorption sites for CH_n fragments

Calculations were performed starting with vertical adsorptions on sites shown in Fig. 3. After optimization, the adsorbates were allowed to move freely on the surface. Adsorbates ad-

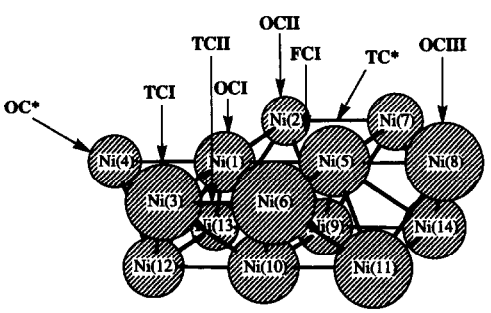

Fig. 3. Modeled nickel surface catalyst. Adsorption sites on a Ni_{15} cluster: one-, two- and four-center sites labeled as OC, TC and FC, respectively.

vance to border sites in which the adsorbate is tilted out from the plane, see TC* and OC* sites indicated in Fig. 3. FCI, TCII and OCII adsorptions move to the TC* site, while TCI, OCI, and OCIII adsorptions shift to OC* one. The bonding properties of C, CH, CH_2, and CH_3 adsorption on OC* and TC* sites are presented in Table 1.

The analysis of the results for different adsorbates show the following trends:

(1) Adsorption of the fragments studied (CH_n, $n = 0, 1, 2, 3$) takes place mainly on border sites, where Ni atoms have the smallest coordination number. The comparison of DBE(C–H) values for free fragments (−84, −88, and 96 kcal/mol for CH, CH_2 and CH_3, respectively) with respect to those of fragments chemisorbed on OC* (average values of −101, −95 and −97 kcal/mol, respectively) reveals a reinforcement of the C–H bond. According to this behavior, and the fact that C–H bond formation is energetically favored with respect to Ni–H one (−69.2 kcal/mol [28]), it is possible to infer that OC* sites (cluster corners) are good sites for hydrogenation of CH_n fragments. This conclusion is in agreement with experimental work [29] that reports that single atoms on the metal surface catalyst are the active sites in alkene hydrogenation reactions.

(2) Electronic charge transfer from the cluster to the CH_n adsorbate takes place upon C chemisorption, which is consistent with the greater electronegativity of the C atom with respect to the Ni atom.

(3) The most stable spin multiplicity of the isolated Ni_{14} cluster was 17 [1], so, the results of the most stable multiplicities for $Ni_{14}CH_n$ systems reveals that CH_n chemisorption produces a reduction of the surface magnetism (see values in parentheses in first row of Table 1). These results are in agreement with experimental findings [30], where interactions of hydrocarbons with a Ni surface yield a diminution of the magnetic moments.

(4) The adsorption in the most stable sites (OC* and TC*) clearly shows: (a) The EBD(Ni–C) values increase with the number of hydrogens of the adsorbed CH_n fragment. (b) In all cases, TDBE(Ni–C), Charge(CH_n), and DBE(C–H) absolute values for the one-center site are larger than for the two-center one.

3.2. Hydrogenation of molecular fragments

As mentioned above, edge sites are the most adequate for hydrogenation; therefore, calculations of a CH_n ($n = 0$–3) fragment plus a H atom adsorbed on edge sites were carried out [31]:

$$CH_n(ad) + H(ad) \rightarrow CH_{n+1}(ad)$$

The results of reactions that lead to hydrogenation of CH_n fragments are shown in a

Table 1
Adsorption properties of C, CH, CH_2 and CH_3 on Ni_{14} cluster optimal sites (TC* and OC*), shown in Fig. 3

System properties	Fragment [a]/optimal sites							
	C (15)		CH (16, 14)		CH_2 (15)		CH_3 (16)	
	TC*	OC*	TC*	OC*	TC*	OC*	TC*	OC*
TDBE (Ni–C) (kcal/mol)	−49.9	−64.9	−72.8	−91.4	−77.2	−87.1	−78.3	−81.8
Charge (CH_n) (au)	−0.214	−0.353	−0.221	−0.332	−0.260	−0.366	−0.229	−0.374
EBD (Ni–C) (Å)	2.058	1.870	2.081	1.894	2.160	1.924	2.161	1.959
			2.110				2.166	
DBE (C–H) (kcal/mol)					−83.5	−90.3	−96.1	−98.5
	—	—	−81.4	−101.1			−84.1	−96.1
					−94.9	−99.5	−84.2	−96.1

TDBE = Total diatomic binding energy. EBD = Equilibrium bond distance.
[a] Values in parentheses are spin multiplicities.

schematic way in Fig. 4. A situation in which a single carbon atom is located on an OC * site in $Ni_{(8)}$ and a hydrogen atom put on-top of a $Ni_{(8)}$ atom leads to the formation of C–H. That is, the hopping of an adsorbed H atom from a neighbor site to OCIII produces CH. The final state for this reaction corresponds to a CH fragment adsorbed on OC *, as shown in Fig. 4a, with a Ni–C–H bond angle lower than 180°. This bending geometry has been reported by Demuth and Ibach [32] on a Ni(111) surface. A similar result is obtained for the situation in which C is adsorbed on TC * and H on OCII ($Ni_{(6)}$) (see last row values in the table inserted in Fig. 4a).

The hydrogenation of methyne was explored in the same site of C adsorption (OC *) but with H on TCl. The final result corresponds to CH_2 chemisorbed on OC *, see Fig. 4b. The results of DBE(C–H) show some differences among the C–H bonds. The reason for this is the small binding interaction of one of the H with $Ni_{(8)}$ and $Ni_{(5)}$ surface atoms. Similar results were obtained starting with CH on TC * and H on OCII (see values in third row of the table included in Fig. 4b).

In the case of methylene, several tests were performed. Only one of them leads to the formation of a methyl radical adsorbed in bridge edges (TC *), as shown in Fig. 4c. The initial location corresponds to CH_2 adsorbed on TC * and H on OCII. The methyl radical presents interactions H–Ni of −5 and −9 kcal/mol for the two H atoms closer to the surface.

All of the above reactions are energetically favored. This is not the case for methane formation, which is more difficult. Vertical adsorptions of CH_3 and H in adjacent sites yields methane, but with 13 kcal/mol less stable than the reactants. The methane molecule is completely distorted and the C–H bonds close to the surface are highly activated, see Fig. 4d. The interaction Ni–C is relatively small and there are also H–Ni bonding interactions of about −12 kcal/mol. These results and the fact that the separated systems (CH_4 + cluster) are more stable than the attached ones, suggest that methane is desorbed once it is formed.

Previous calculations [1,3] suggest that edge sites in the model nickel cluster are the most populated with hydrogen, because there the H_2

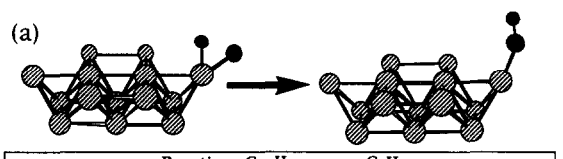

Reaction: C + H-------->C-H

Initial Sites	Final Sites	EBD(C-H) Å	EBD(C-Ni) Å	DBE(C-H) kcal/mol	DBE(C-Ni) kcal/mol
C-(OC*) + H-(OCIII)	HC-(OC*)	1.118	1.885	-90.9	-79.4
C-(TC*) + H-(OCII)	HC-(OCII*)	1.124	1.928	-95.8	-79.1

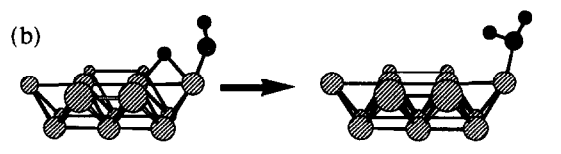

Reaction: CH + H-------->HC-H

Initial Sites	Final Site	EBD(C-H) Å	EBD(C-Ni) Å	DBE(C-H) kcal/mol	DBE(C-Ni) kcal/mol
HC-(OC*) + H-(TCl)	H_2C-(OC*)	1.115 1.151	1.913	- 99.5 - 79.4	-83.8
HC-(TC*) + H-(OCII)	H_2C-(OCII*)	1.124 1.155	1.915	- 99.6 - 80.6	-79.4

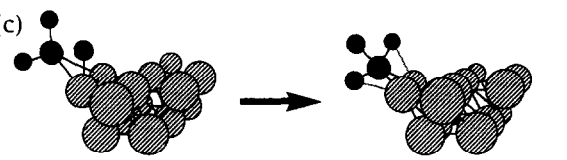

Reaction: CH_2 + H -------> CH_3

Initial Sites	Final Site	EBD(C-H) Å	EBD(C-Ni) Å	BE(C-H) kcal/mol	BE(C-Ni) kcal/mol
H_2C-(TC*) + H-(OCII)	H_3C-(TC*)	1.160 1.134 1.164	2.170 2.105	- 80.0 - 96.4 - 79.3	- 35.9 - 45.0

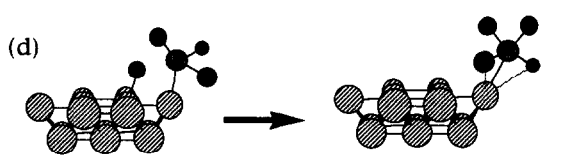

Reaction: CH_3 + H -------> CH_4

Initial Sites	Final Site	EBD(C-H) Å	EBD(C-Ni) Å	DBE(C-H) kcal/mol	DBE(C-Ni) kcal/mol
H_3C-(OCIII) + H-(OCI)	HC_4-(OC*)	1.13 1.13 1.24 1.25	2.08	- 97.1 - 97.4 - 48.9 -58.8	- 48.4

Fig. 4. Surface hydrogenation reactions: $CH_n + H \rightarrow CH_{n+1}$ ($n = 0$–3). The binding properties presented in inserted tables correspond to the final state.

is dissociated, due to the strong Ni–H binding interaction. Then, because these sites are also the most active for hydrogenation, a situation in which the number of CH_n is smaller than the number of H_2 molecules (i.e., high hydrogen pressure) will be the case in which hydrogenation is favored. On the other hand, when the concentration of CH_n fragments is high, the edge sites are occupied with these fragments, leading to a strong relaxation of Ni–Ni bonds. In this case, the chemisorption of the CH_n fragments on four-center sites becomes the most important. The interaction of CH_n fragments in these sites shows significant C–H activation [33], favoring the dehydrogenation process. For example, calculations of interactions of four CH_2 fragment with a Ni_5 cluster [33] reveal an important cluster relaxation that provokes a strong chemisorption of a fifth CH_2 on the four-center site, with a weak C–H bond (DBE(C–H) of −36 kcal/mol). The change in adsorption surface properties (more active FC sites), due to chemisorption of CH_n fragments on edges, can be interpreted as a 'cooperative effect'. A like effect has been used to explain the C diffusion into the Ni cluster [34] through FC sites.

3.3. Hydrocarbon formation

The main product in the hydrogenation of carbon is methane, although it is also possible that CH_n intermediates react to yield longer hydrocarbon chains, as suggested in various studies [24,35].

Dimerization reactions between fragments to form larger hydrocarbons were also performed [31] on the Ni cluster adsorption sites, shown in Fig. 3. The formation of acetylene and ethylene is presented in a schematic way in Fig. 5a and b.

Two CH fragments located on TC * and OCII site lead to the formation of acetylene, as depicted in Fig. 5a. The results of DBE (−134.1 kcal/mol) and EBD (1.331 Å) show that the C–C bond is intermediate between single

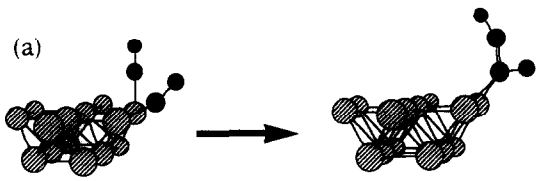

Reaction: CH + CH -------> HC-CH					
Initial Site	Final Site	EBD(C-C) Å	EBD(C-Ni) Å	DBE(C-C) kcal/mol	DBE(C-Ni) kcal/mol
HC-(TC*) + HC-(OCI)	H_2C_2-(TC*)	1.331	2.260 2.168	-134.1	-33.2 -42.1
HC-(OCIII) + HC-(OCI)	H_2C_2-(OC*)	1.309	1.984	-155.6	-80.4

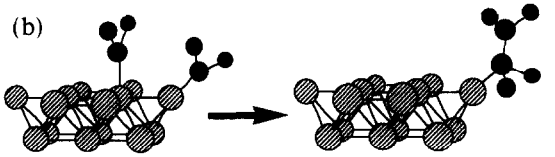

Reaction: $CH_2 + CH_2$ -------> $H_2C\text{-}CH_2$					
Initial Site	Final State	EBD(C-C) Å	EBD(C-Ni) Å	DBE(C-C) kcal/mol	DBE(C-Ni) kcal/mol
H_2C-(OCI) + H_2C-(OCIII)	C_2H_4-(OC*)	1.463	1.994	-104.0	-78.2

Fig. 5. Dimerization reactions: $CH_n + CH_n \rightarrow C_2H_{2n}$ ($n = 1, 2$). The binding properties presented in inserted tables correspond to the final state.

(−100.2 kcal/mol and 1.487 Å) and double bonds (−157.6 kcal/mol and 1.321 Å) of C_2H_6 and C_2H_4 calculated molecules. Note that the C atom is bonded to two Ni atoms on the surface. The formation of C_2H_2 is favored in these sites, because a strong C–C bond is formed (−134 kcal/mol), while a weaker Ni–C bond is broken (−75 kcal/mol). A strong chemisorption of C_2H_2 resulted for the interaction of two adjacent CH fragments adsorbed on one-center sites (OC * and OCI). Because the C atom is bonded to only one Ni atom, then the EBD(C–C) (1.309 Å) and DBE(C–C) (−156 kcal/mol) are very close to a double bond.

Adsorbed ethylene is produced when two CH_2 are chemisorbed on OC * and OCI sites, see Fig. 5b. The EBD and DBE for C–C bond shows the characteristic of a single bond. A similar conformation as C_2H_2 is observed; i.e., the C–C is almost perpendicular to the surface. The formation of C_2H_4 is less favored than in the case of acetylene because the C–C bond formed is weaker. Calculations for two CH_3 groups were also carried out, however, C_2H_6 was not formed.

3.4. Formation of carbonaceous chains

Calculations of the interaction between CH fragments (the most common fragment in hydrocarbon decomposition reactions on nickel surfaces [36]) and adsorbed carbon atoms have been carried out [37]. The starting point was selected assuming partially saturated edge sites; i.e., adsorption on OCIII and OCII sites, and adsorption of C atoms on FC and OCI sites, see Fig. 6. The initial carbon–surface distances were obtained from calculations of a single C–H fragment [33], in the respective site. Calculations were performed by optimizing only the geometrical coordinates of the C and H atoms and considering also different multiplicities. The results for the most stable multiplicity, 11, are shown in Fig. 6.

Several features can be noticed from the analysis of Fig. 6 and the table included: (a) The interaction of several fragments of CH and C leads to the formation of partially hydrogenated carbonaceous structures with a Ni–C interaction of −51 kcal/mol. (b) the most stable CH fragments adsorbed on OCIII sites (atoms Ni(8) and Ni(4)) stay in the same site, but are tilted outward from the surface with strong Ni–C bonds of −88 to −93 kcal/mol. (c) One of the CH fragments adsorbed on OCII sites is inserted into the C–Ni bond of the adjacent CH; for example, H(27)–C(17) adsorbed on Ni(6) is included in the Ni(3)–C(19) bond. (d) C atoms on OCI and on FC are displaced from the surface to form a 4-member ring with an average DBE(C–C) per bond of −91 kcal/mol.

These results show that some C and C–H fragments adsorbed on a nickel surface are able to produce small polymeric species, which may be precursors of large polymeric chains, filamental, and graphitic carbons, as has been proposed by Jackson et al. [38].

4. Active site for H_2 dissociation in HDS, HDN and HDM reactions

Hydrodesulfurization (HDS), hydrodenitrogenation (HDN), hydrodemetalization (HDM) are processes for the removal of S, N, and metals, respectively. Several industrial catalysts used in these processes are based on molybdenum disulfide (MoS_2) anchored on a support.

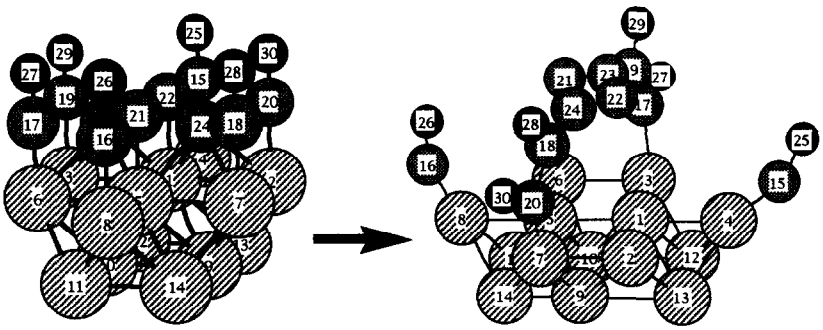

X-Y Bond	DBE(X-Y) kcal/mol	X-Y Bond	DBE(X-Y) kcal/mol	X-Y Bond	DBE(X-Y) kcal/mol
Ni(8)-C(16)	-88.1	C(18)-C(24)	-102.4	C(22)-C(23)	-92.0
Ni(4)-C(15)	-93.0	C(24)-C(22)	-92.4	C(19)-C(23)	-103.0
Ni(3)-C(17)	-51.3	C(24)-C(21)	-87.2	C(19)-C(17)	-134.2
Ni(7)-C(20)	-51.3	C(21)-C(23)	-91.0	C(X)-H(X)	-94.4
C(20)-C(18)	-134.0	C(21)-C(22)	-41.2		

Fig. 6. Formation of carbonaceous chains: 6CH + 4C → C_8H_4 + 2CH. The binding properties presented in the inserted table correspond to the final state.

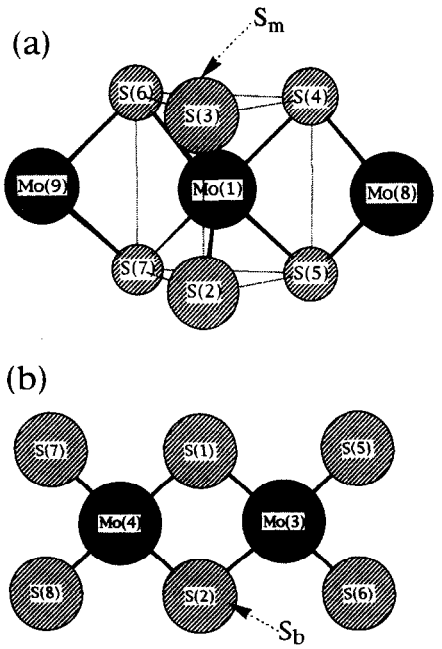

Fig. 7. Clusters with monocoordinated (S_m) and bicoordinated (S_b) sulfur atoms. (a) Mo_3S_6 and (b) Mo_2S_6.

The activity of this type of catalyst depends on the capacity of dissociating H_2 to form –SH groups which react later to yield H_2S, leading to the formation of vacancies on the metallic atoms. Therefore, as has been stated in the literature [39–41], the understanding of how and where these –SH groups are formed is essential in order to model new materials for these types of catalytic processes.

According to the literature, the active sites for the HDS reaction are located at the edge of small MoS_2 crystallites. Wambeke et al. [40] suggest that at the first stage of the activation of the MoS_2/γ-Al_2O_3 catalyst, the monocoordinate sulfur atoms (S_m) at the surface are eliminated, leading to Mo sites with vacancies. This result is supported by Diemann et al. [41] who propose that strongly unsaturated active sites are formed on the edges of a MoS_2-like crystallites.

To study the characteristics of the active sites for dissociation of H_2 and the formation of –HS groups on a MoS_2 surface, calculations [20,21] were performed with Mo_3S_6, Mo_2S_6, (see Fig. 7) $Mo_3S_6H_2$ and $Mo_2S_6H_2$ clusters, using the Effective Core Potential (ECP) of the HONDO-8 program [42]. Semi-core ECP was employed for the Mo atom, as proposed in a previous work [20,21]. The critical points of $\Delta\rho(\mathbf{r})$ and the Bader's electronic charges were calculated with a modified version of the EXTREM program [43] and with the PROAIM program [44], respectively.

4.1. Critical points at the sulfur valence shell

As mentioned in Section 2.3, the critical points of $\Delta\rho(\mathbf{r})$ at the valence region offer a description of the places where valence electronic charges are concentrated or depleted [16,18,28], in other words, the active sites can be mirrored by the $\Delta\rho(\mathbf{r})$ topology.

In order to study the location of active sites for H_2 dissociation on a modeled MoS_2 surface, the CPs at the sulfur valence region were evaluated [20,21] on S_m and S_b atoms (monocoordinated and bicoordinated, respectively) of Mo_3S_6

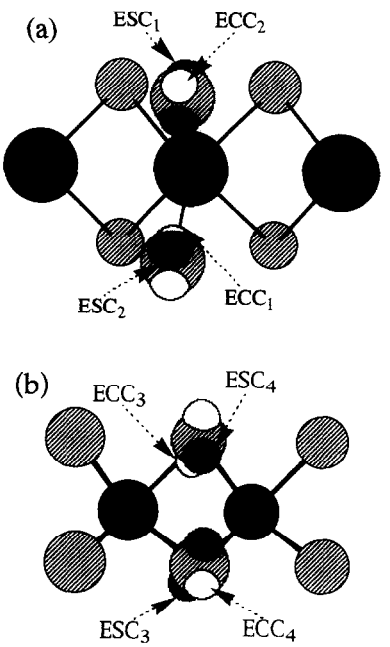

Fig. 8. Schematic representation of $\Delta\rho$ and $\Delta\rho_{spin}$ CP locations on the valence shell of (a) Mo_3S_6 and (b) Mo_2S_6 clusters. ECC and ESC are electronic charge and spin concentrations, respectively.

and Mo_2S_6 clusters. Beside the topological properties of $\Delta\rho(r)$, an analysis of $\Delta\rho_{spin}(r)$ ($\rho_{spin}(r) = \rho_\alpha(r) - \rho_\beta(r)$) was also carried out. A schematic representation of the location of (3, −3) CPs of $\Delta\rho(r)$ and $\Delta\rho_{spin}(r)$ shown in Fig. 8 for Mo_3S_6 and Mo_2S_6 clusters, as electronic charge concentration (ECC_i) and electronic spin concentration (ESC_i) ($i = 1$–4), respectively. The values of $\rho(r)$ and $\Delta\rho(r)$ at CPs are displayed in Table 2. According to the results ($\Delta\rho(r) < 0$ and $\Delta\rho_{spin}(r) < 0$), as expected, these CPs correspond to sites where there is electronic charge and electronic spin concentration, respectively. These accumulations of charge and spin are in the same plane but one is perpendicular to the other, see white and black half-spheres in Fig. 8, for ECC and ESC, respectively.

4.2. Dissociation path for H_2 molecule

To study the activity of the ECC_2 and ECC_4 CPs for H_2 dissociation on Mo_3S_6 and Mo_2S_6 clusters, different approaches of H_2 to S_m and S_b atoms were considered (the H–H, CP and the S atom are in a line; the H–H is perpendicular to the CP–S line). For these paths H_2 dissociation was not reached. This may be explained by a high repulsion between the electronic charge concentration at the S atom and the closed shell of the H_2 molecule. In addition, the electronic density associated with the ECC_2 and ECC_4 points is strongly bonded to the S atom, and therefore, is not reactive.

Other calculations were carried out moving H_2 close to spin density Laplacian CPs (ESC_2 and ESC_4). The H_2 molecule was parallel to the line that joined two ECC_2 or two ESC_4 CPs, see Fig. 8. The H_2 laid in the plane CP–S–S. Calculations show that H_2 is dissociated, Producing two –SH groups. This result can be explained by analyzing the energy of the electronic density associated with ESC_2 or ESC_4. Because this density corresponds to unpaired electrons, it must be related with HOMO orbitals. These are less stable that those densities that compose the ECC_2 and ECC_4, and therefore, an electronic charge density transfer may occur from ESC_2 or ESC_4 to the antibonding H_2 σ^* orbital, leading to H–H dissociation. Another feature facilitates this transfer: the electron–electron repulsion between ESC_2 or ESC_4 and σ occupied orbital is less than in the cases of ECC_2 and ECC_4, because $\rho_{spin}(r)$ is much smaller than $\rho(r)$, see values in the last column of Table 2.

Table 2
Values of $\Delta\rho(r)$ and $\rho(r)$ at the S valence shell (3, −3) CP for Mo_3S_6 and Mo_2S_6 clusters [a]. ECC and ESC mean electronic charge concentration and electronic spin concentration, respectively, see Fig. 8

Cluster	CP	$\Delta\rho(r)$	$\rho(r)$	CP	$\Delta\rho(r)$	$\rho(r)$
Mo_3S_6	ECC_1	−0.844	0.182	ECC_2	−0.936	0.187
Mo_2S_6	ECC_3	−0.877	0.186	ECC_4	−0.969	0.193
Mo_3S_6	ESC_1	−0.471	0.073	ESC_2	−0.406	0.065
Mo_2S_6	ESC_3	−0.338	0.052	ESC_4	−0.351	0.051

[a] All values in atomic units.

One should notice that the determination of spin concentration densities on surface atoms may facilitate the localization of the optimal places for chemisorption and dissociation of the H_2 molecule. This feature is of great importance, because it may help to save much time in quantum mechanical calculations that require the optimization of adsorbate–surface interactions, starting from different points and different orientations of the adsorbate.

5. The mechanism of HDN reaction

The presence of N-compounds leads to the poisoning of hydrocracking and reforming catalysts in the later stages of oil refining. In addition, the decomposition of these compounds causes NO_x pollution of the atmosphere. In recent years, due to more severe rules of environmental protection agencies, hydrodenitrogenation is becoming a process of prime importance in the oil industry in order to lower the nitrogen content of petroleum products.

A single MoS_2 layer represents a reasonable model for this catalyst because the electronic inter-layer interaction is relatively weak [45]. In related work, synthesized linear clusters of molybdenum and sulfur have been used as precursors of HDS catalysts [46] and as molecular models of MoS_2 [47]. Here, we show the results of modeling the interaction of a model molecule (pyridine) that represent an N-compound with a hydrogenated surface of MoS_2 catalyst represented by a $Mo_3S_8H_2$ cluster [48]. In this case, a modified CNDO-UHF [49] method was employed.

The bonding interactions between the pyridine and the hydrogenated surface were analyzed by using total energy, Mulliken bond orders (MBO), diatomic energies (DE), overlap and orbital coefficients of interacting atoms, and Mulliken charges densities. These variables were used for studying the relative stability of adsorption on different active sites, bonding modes, activation of C–C, C–H, and C–N bonds, formation of C–H bonds, Mo-pyridine bonding interactions, and net charge transfers.

The HDN reaction occurs essentially through a two-step process: first, the aromatic ring is saturated with hydrogens; and second, the removal of nitrogen through a C–N bond cleavage by hydrogenolysis. Details of the HDN mechanism have not been clearly established yet.

Calculations of pyridine adsorption on a hydrogenated surface ($Mo_3S_8H_2$) were carried out [48] in order to understand the first step of hydrogenation. To select the H locations, calculations of H interaction with several adsorption sites were studied, the Mo–Mo bridge sites being the most stable ones. A previous study of pyridine interaction with Mo_3S_8 cluster [50] revealed that interactions with on-top sites are the most favored. Therefore, the pyridine interaction with $Mo_3S_8H_2$ was calculated considering various adsorption modes (π and σ) with on-top site, as shown in Fig. 9 for systems I–III. Several multiplicities were considered, the quintuplet being the most stable one.

An analysis of the overlap between adsorbate and surface orbitals and the corresponding molecular orbital coefficients leads to a description of the different types of interactions involved in the chemisorption and the hydrogenation process. A schematic picture of the atomic orbital interactions of pyridine carbon and nitrogen atoms with metallic atoms (Mo(1) and Mo(2)) and adsorbed hydrogens with pyridine carbon atoms are shown in Fig. 10a, b. Note the appearance of a strong interaction H(ads)–pyridine.

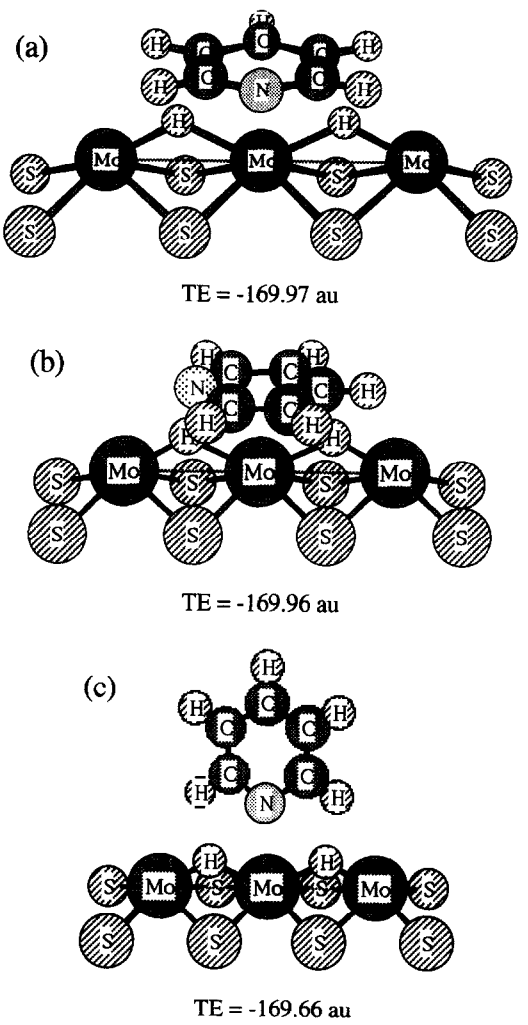

Fig. 9. Pyridine adsorption on $Mo_3S_8H_2$ in: (a) System I (π-mode adsorption with pyridine C_3–N axis perpendicular to Mo–Mo line). (b) System II (π-mode adsorption with pyridine C_3–N axis parallel to MoMo line). (c) System III (σ-mode adsorption).

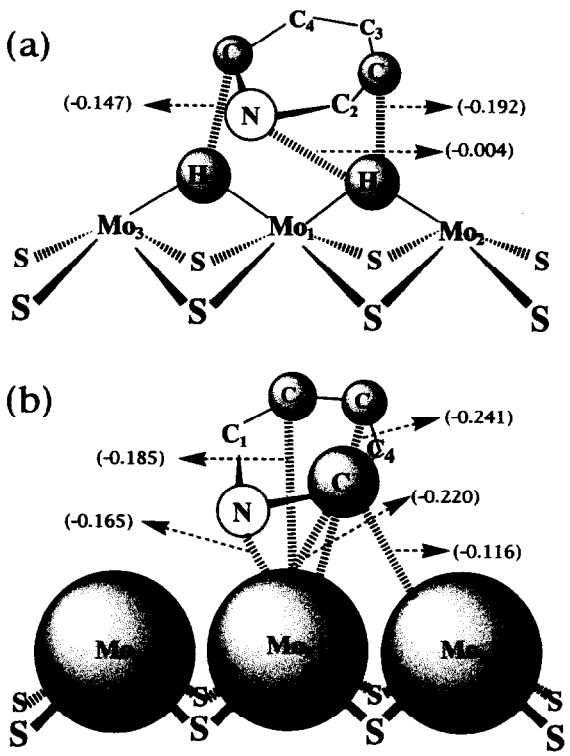

Fig. 10. Interaction of s-orbitals. (a) Adsorbed hydrogens and C and N pyridine atoms. (b) Pyridine atoms (C, N) and Mo atoms of the cluster. Values in parentheses are diatomic energies, in atomic units, of the interacting atoms.

The analysis of the results reveals several interesting facts:

(a) The chemisorption in the π-mode is stronger than in the σ-mode and, therefore, the activation of C–N and C–C bonds in pyridine is greater in π- than in σ-adsorption.

(b) The electron charge transfer occurs from pyridine to Mo_3S_8 cluster. This transfer correlates with the stability of adsorption structures, i.e., more stable systems correspond to more withdrawing of electronic charge from the pyridine to the MoS_2 surface model.

(c) Small direct participation of d orbitals in the bond. It means that the overlap between d orbitals and pyridine atoms is small. The d participation, as has been shown in previous papers [3,4,51], is due to a reorganization of the electronic d cloud, which is the result of a strong electron–nucleus interaction.

(d) The pyridine atoms interact with the metallic atom which is directly below (Mo_1), but also with adjacent atoms (Mo_2 and Mo_3).

(e) Significant interactions between adsorbed hydrogens (H_6 and H_7) and pyridine carbons suggest the hydrogenation of the π-mode adsorbed pyridine on one-center sites.

(f) An important interaction between the pyridine hydrogen atoms (H_2, H_4, H_1, H_5) with adjacent Mo atoms indicates the presence of agostic bonds (i.e., Mo $\cdots$ H–C bond).

(g) The results of system II (see Fig. 9b) show a small energy difference with respect to system I (see Fig. 9a). In addition, the bonding interaction between adsorbed hydrogens with pyridine atoms in the system II (MBO(H_6–N) = 0.707 and MBO(H_7–C_3) = 0.779) is larger than in the system I (MBO(H_7–C_1) = 0.335 and MBO(H_7–C_5) = 0.349). These facts suggest a mechanism for pyridine hydrogenation on a MoS_2 hydrogenated catalyst. The following steps are proposed: (i) adsorption of pyridine in π-coordination mode on a Mo atom. The pyridine is oriented in such a way that a line between N and C_3 atoms is parallel to the Mo–Mo internuclear line. (ii) Hydrogenation of pyridine N and C_3 atoms first occurs, leading to the formation of an intermediate compound with two double bonds. (iii) Rotation of the pyridine in an axis perpendicular to the main plane of the molecule and subsequent hydrogenations.

6. General conclusions

(a) The modeling of hydrotreatment processes is very complex because, as in most of heterogeneous catalysis reactions, several steps are involved, and calculations require the handling of transition metals. The use of model Hamiltonians based on parametric functionals, such as MINDO/SR, CNDO/2, and HF-ECP, are adequate for the treatment of these complicated systems, permitting us to obtain very important qualitative information.

(b) New computational tools that allow calculation of diatomic binding energies and the evaluation of topological properties of ρ and $\Delta\rho$ are very convenient and advantageous for the analysis of bonding properties of adsorbates and to understand the nature of active adsorption sites on a modeled surface.

Acknowledgements

The authors want to acknowledge the contribution of CONICIT (project S1-2690) for providing funds to obtain computer facilities. We thank CYTED V-4 and RED TEMATICA: Química Computacional for allowing the discussion and diffusion of these results. FMP appreciates the financial support given by COPLAC and Colciencias.

References

[1] F. Ruette, G. Blyholder and J. Head, Surf. Sci. 137 (1984) 491.
[2] F. Ruette, G. Blyholder and J.D. Head, J. Chem. Phys. 80 (1984) 2042; F. Ruette, E.V. Ludeña and A.J. Hernández, Int. J. Quantum Chem. XXIX (1986) 1351; F. Ruette and G. Blyholder, Theor. Chim. Acta 74 (1988) 137; L.J. Rodríguez, F. Ruette and M. Rosa-Brussin, J. Mol. Catal. 62 (1990) 199; M. Sánchez, F. Ruette and A.J. Hernández, J. Phys. Chem. 96 (1992) 823.
[3] F. Ruette, A.J. Hernández and E.V. Ludeña, Surf. Sci. 151 (1985) 103.
[4] F. Ruette, E.V. Ludeña, A.J. Hernández and G.R. Castro, Surf. Sci. 167 (1986) 393.
[5] G. Blyholder, J. Head and F. Ruette, Theor. Chim. Acta 60 (1982) 429.
[6] F. Ruette, A. Sierraalta and A. Hernández, in: F. Ruette (Editor), Quantum Chemistry Approaches to Chemisorption and Heterogeneous Catalysis (Kluwer, Dordrecht, 1992) p. 320, and references therein.
[7] P. Durand and J-P. Mairieu, Adv. Chem. Phys. 68 (1987) 321.
[8] P-O. Löwdin, Adv. Quantum Chem. 23 (1992) 83.
[9] M. Romero, J. Primera, M. Sánchez, A. Sierraalta, S. Brassesco, J. Bravo and F. Ruette, Folia Chimica Theoretica Latina, accepted for publication.
[10] M. Romero, J.R. Primera, M. Sánchez, A. Sieraalta and F. Ruette, J. Mathematical Chem., submitted for publication.
[11] R.C. Bingham, M.J.S. Dewar and D.H. Lo, J Am. Chem. Soc. 97 (1975) 1285.
[12] H. Kollmar, Theor. Chim. Acta 50 (1978) 235; M. Sanchez and F. Ruette, J. Mol. Struct. (Theochem) 254 (1992) 335.
[13] R.S. Mulliken, J. Chem. Phys. 23 (1955) 1841.
[14] F. Ruette, F.M. Poveda, A. Sierraalta and J. Rivero, Surf. Sci. 349 (1996) 241.
[15] I. Meyer, in: Z.B. Maksic (Editor), Modeling of Structure and Properties of Molecules (John Willey, New York, 1987) p. 147; A. Sierraalta and G. Frenking, Theor. Chim. Acta, submitted.
[16] R.F.W. Bader, Atoms in Molecules: A Quantum Theory (Clarendon Press, Oxford, 1990).
[17] R.F.W. Bader, R.J. Gillespie and P.J. MacDougall, J. Am. Chem. Soc. 110 (1988) 7329; R.J. Gillespie, Can. J. Chem. 70 (1992) 742; R.F.W. Bader, Molecules in Physics, Chemistry and Biology, Vol. III (Kluwer Academic Publishers, 1989) p. 73; R.F.W. Bader, P.L.A. Popelier and C.J. Chang, J. Mol. Struct. (Theochem) 255 (1992) 145.
[18] R.F.W. Bader, Chem. Rev. 91 (1991) 893.
[19] Y. Aray, J. Rodriguez, J. Murgich and F. Ruette, J. Phys. Chem. 97 (1993) 8393; Y. Aray, F. Rosillo and J. Murgich, J. Am. Chem. Soc. 116 (1994) 10639; Y. Aray and J. Rodríguez, Can. J. Chem. 74 (1996) 1014; Y. Aray and R.F.W. Bader, Surf. Sci. 31 (1996) 233.
[20] A. Sierraalta and F. Ruette, J. Comp. Chem. 15 (1994) 313; A. Sierraalta and F. Ruette, Int. J. Quantum Chem. 60 (1996) 1015.
[21] A. Sierraalta and F. Ruette, J. Mol. Catal. 109 (1996) 227.
[22] I.M. Campbell, Catalysis at Surfaces (Chapman and Hall, London, 1988) p. 75.
[23] J.T. Yates, S.M. Gates and J.N. Russell, Surf. Sci. 164 (1985) L839; C.K. Rofer De Poorter, Chem. Rev. 81 (1981) 457; P. Biloen, J.N. Helle and W.M.H. Sachtler, J. Catal. 58 (1979) 102.
[24] R.C. Brady and R. Petit, J. Am. Chem. Soc. 103 (1981) 1287.
[25] M.P. Kaminsky, N. Winograd and G.L. Geoffroy, J. Am. Chem. Soc. 108 (1986) 1315.
[26] H. He, J. Nakamura and K. Tanaka, Surf. Sci. 283 (1993) 117.
[27] S. Tjandra and F. Zaera, J. Vac. Sci. Technol. A 10 (1992) 404.
[28] R.F.W. Bader and H. Essen, J. Chem. Phys. 80 (1984) 1943; R.F.W. Bader, P.J. MacDougall and C.D.H. Lau, J. Am. Chem. Soc. 106 (1984) 1594.
[29] P.S. Kirlin and B.C. Gates, Nature (London) 325 (1987) 38.
[30] G.A. Margin and B. Imelik, Surf. Sci. 42 (1992) 157; J. Erkelens and W.J. Wösten, J. Catal. 54 (1978) 143.
[31] F.M. Poveda, J.L. Villaveces and F. Ruette, to be published.
[32] J.E. Demuth and H. Ibach, Surf. Sci. 78 (1978) L238.
[33] F.M. Poveda and F. Ruette, to be published.
[34] F.M. Poveda and F. Ruette, J. Mol. Catal. 106 (1966) 109.
[35] R.D. Kelley and S. Semancik, J. Catal. 84 (1983) 248; R.W. Joiner, J. Catal. 50 (1977) 176.
[36] S.T. Ceyers, Langmuir 6 (1990) 82; D.W. Goodman, R.D. Kelley, L.E. Madey and J.L. Yates, J. Catal. 63 (1980) 226.
[37] F. Ruette and F.M. Poveda, in: Electron Processes at Solid Surfaces (World Scientific Publishing Co.), in press.
[38] S.D. Jackson, S.J. Thomson and G. Webb, J. Catal. 70 (1981) 249.

[39] A.L. Dicks, R.L. Ensell, T.R. Phillips, A.K. Szczepura, M. Thorley, A. Williams and R.D. Wragg, J. Catal. 72 (1981) 266; J.M.J.G. Lipsch and G.C.A. Schuit, J. Catal. 15 (1969) 179; H. Kwart, G.C.A. Schuit and B.C. Gates, J. Catal. 61 (1980) 128; J. Barbour and K. Campbell, J. Chem. Soc. Chem. Commun. (1982) 1371; M. Vrinat, M. Breysse, C. Geantet, J. Ramirez and F. Massoth, Catal. Lett. 26 (1994) 25; B. Delmon and J.L. Dallons, Bull. Soc. Belg. 97 (1988) 473; T.F. Hayden and J.A. Dumesic, J. Catal. 103 (1987) 366.

[40] A. Wambeke, L. Jalowiecki, S. Kasztelan, J. Grimblot and J.P. Bonnelle, J. Catal. 109 (1988) 320.

[41] E. Diemann, Th. Weber and A. Müller, J. Catal. 148 (1994) 288.

[42] MOTECC-90™, IBM Corporation Center for Scientific and Engineering Computation, Kingston, N.Y., U.S.A. (1990).

[43] R.F.W. Bader, Department of Chemistry, McMaster University, Hamilton, Ontario, Canada (1994).

[44] F.W. Biegler-Konig, R.F.W. Bader and T.H. Tang, J. Comp. Chem. 3 (1982) 317.

[45] A. Wold and K. Dwight, Solid State Chemistry (Chapman and Hall, New York, 1993) p. 186.

[46] A. Müller, E. Diemann, A. Branding, F.W. Baumann, M. Breysse and M. Vrinat, Appl. Catal. 62 (1990) L13.

[47] A. Müller, Polyhedron 5 (1986) 323.

[48] E.N. Rodriguez-Arias, A.E. Gainza, A.J. Hernández, P.S. Lobos and F. Ruette, J. Mol. Catal. 102 (1995) 163.

[49] J.A. Pople and D.L. Beveridge, Approximate Molecular Orbital Theory (McGraw-Hill, New York, 1970); D. Rinaldi, GEOMO Program, QCPE, No. 290 (1976); A.J. Hernández, F. Ruette and E.V. Ludeña, J. Mol. Catal. 39 (1987) 21; H. Castejón, A.J. Hernández and F. Ruette, J. Phys. Chem. 92 (1988) 4970.

[50] A.E. Gainza, E.N. Rodríguez and F. Ruette, J. Mol. Catal. 85 (1993) 345.

[51] L.J. Rodríguez, F. Ruette, G.R. Castro, E.V. Ludeña and A.J. Hernández, Theor. Chim. Acta 77 (1989) 39.